Slot-waveguide Analysis and Fabrication of a Planar Dielectric Waveguide

Author: David Sánchez Gonzalo.

Facultat de Física, Universitat de Barcelona, Diagonal 645, 08028 Barcelona, Spain*.

Abstract: Waveguides are present in many devices for communication, but this work tries to deal with their application in optical biosensing. First, a theoretical treatment is carried out with the objective to describe the demeanour of two biosensor systems, dielectric waveguide biosensor and novel waveguide geometry for enhancing and confining light named slot-waveguide. This last configuration will be explained more widely and analysing the results of different simulations. Finally, planar and rib multimode waveguides on SU8 polymer has been fabricated. Prism coupling has been used as insertion of light and, finally, the number of guided modes has been measured.

I.   INTRODUCTION

A waveguide is a region of space, with a defined geometry, where an electromagnetic wave can be confined and propagated with low losses. This mechanism is useful in some applications. On the one hand, a big number of devices for optical communications: optical couplers [1], Mach-Zender modulators [2], phase and amplitude modulators, active layer of semiconductor lasers, etc. On the other hand, the application of waveguides in optical biosensing: Mach-Zender interferometer biosensors [3], resonant coupling biosensing etc. Conventional strip and rib waveguides are commonly used in biochemical sensors based on integrated optics. Usually the guiding mechanism is based on total internal reflection (*TIR*) and the confinement of light in a high-index material (*core*) surrounded by a low-index material (*cladding*). Other type of structures exist where the light propagates in a low index material: i) ARROW (AntiResonantOpticalWaveguides) waveguides, thanks to the high reflective of specific layers in the structure [3] and ii) slot waveguides, that is the purpose of this work [4].

II.   PHYSICAL CONFINEMENT OF LIGHT FOR BIOSENSING

The working principle of optical waveguide sensors is generally based on the perturbation of the electromagnetic waves of a guided mode caused by optical absorptions, fluorescence or refractive index changes of measurands in the surface. Thus, from the standpoint of which part of the electromagnetic wave interact with the sample, classically are roughly classified into evanescent-wave (those extending to cladding) sensors. But recently a new guided-wave system has been discovered named slot-waveguide. This work describe an example of confinement light in waveguide and their use for an evanescent-wave sensor, and in a way more widespread this new type of biosensor called slot-waveguide.

A.   Dielectric waveguides

The underlying principle of optical confinement is simple. A medium of refractive index n_1, embedded in a medium of lower refractive index $n_2 < n_1$, acts as a light "trap" within which optical rays remain confined by multiple total internal reflections at the boundaries illustrated in figure 1.

The condition for the guiding inside de core is that the incident angle must be below a critical one, $\theta_i < \theta_c$, with an easy expression: $\sin(\theta_i) < \sin(\theta_C) = \sqrt{\epsilon_2/\epsilon_1} = n_2/n_1$.
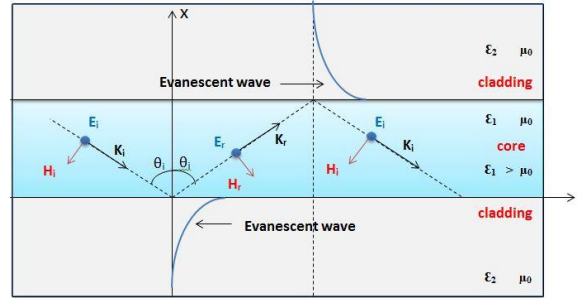

FIG 1: Total internal reflection in a dielectric waveguide, where θ_i is the incident angle and $\epsilon_{1,2}$ are the permittivity of the material which if it is considerate a perfect dielectric, $\epsilon_{1,2} = n_{1,2}^2$. Fields correspond to TE (Transversal Electric) mode.

For that case, EM field shows an ondulatory profile with a decay evanescent wave (*EW*) at the cover and substrate ($\propto e^{-\alpha x}$) in the interface with the core, due to the conservation of the momentum of light and involving the Poynting vector. The EW is defined by (1)

$$E(x) = E_0 e^{-\alpha x} \qquad (1)$$

$\alpha = 1/\delta$ is the attenuation coefficient and δ stands for the penetration depth, defined as (2)

$$\delta = \frac{\lambda}{2\pi n_1 \sqrt{n_1^2 \sin^2 \theta_i - n_2^2}} \qquad (2)$$

Penetration depth is the distance that the amplitude of the EM (E_0), diminishes in a $1/e$ factor in the external medium. This last parameter is very important when optical waveguides are used for biosensors, because it defines the distance that the EW remains enough power, and the molecules that may further than this penetration depth, cannot be sensed. Moreover, it is desired that the confinement is not too efficient, and so the EW is large (figure 2). Normally, δ is around 100nm, enough for detection of proteins, and antibodies.
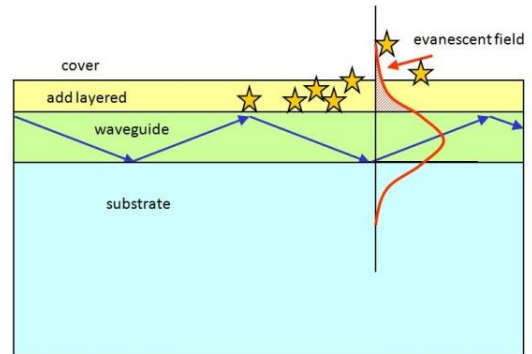

FIG. 2: Optical waveguide working as a biosensor with an add layered which contain the measurands (yellow stars).

---

*Electronic Address: dsartiom@gmail.com

Evanescent field biosensors are selective, because their surface are functionalized with a specific antibody in order to bind with the specific molecules to detect (antigen) present in the analyte. When molecules are attached, the adlayer growth and change the propagation conditions of light. One important application is the measurement of kinetics of molecular reactions [5].

B. Slot confinement analysis

A novel guided-wave configuration, known as a slot-waveguide, was introduced in 2004. This structure is able to guide and strongly confine light in a nanoscale low-refractive index material by using TIR at levels that cannot be achieved with conventional waveguides. It consists of two strips (rails) of high refractive index (n_H) separated by a low-index (n_S) region (slot) of width w_{slot}. Usually, evanescent biosensors works with TE polarization, where electric filed is parallel to both interfaces (figure 1), by contrast, the slot waveguides work in TM polarization. In any polarization, tangential components of E and H must be continuous, and in slot waveguides results in a discontinuity of electrical field with higher amplitude in the low-index region. This discontinuity can be used to strongly enhance and confine light in a nanometer-wide region of low-index material. The principle of operation of this structure can be illustrated by analysis of the structure shown in figure 3a, where a low index material (n_s = slot) is embedded between two guides with higher refraction index (n_H), (shaded region).

The analytical solution for the transverse E-field profile Ex of the fundamental TM eigenmode of the slab-based slot waveguide is shown in equation (3) [6]. Where κ_H is the transverse wave number in high refractive index slabs, γ_C and γ_S are the field decay coefficient in the cladding and in the slot respectively. Constant A can be narrated mathematically as follows (4):

$$A = A_0 \frac{\sqrt{k_0^2 n_H^2 - \kappa_H^2}}{k_0} \quad (4)$$

A_0 is an arbitrary constant, and $k_0 = 2\pi/\lambda_0$ is the vacuum wave number. This A constant is not calculated because the subsequent treatment of the EM field will be normalized and divided by A, so that constant doesn't appear in the calculus.

The transverse parameters are interrelated by the β parameter like the following expression shown (5)

$$k_0^2 n_H^2 - \kappa_H^2 = k_0^2 n_C^2 + \gamma_C^2 = k_0^2 n_S^2 + \gamma_S^2 = \beta^2 \quad (5)$$

where β is the eigenmode propagation constant, and it is obtained by solving the transcendental characteristic equation (6)

$$\tan[\kappa_H(b-a) - \phi] = \frac{\gamma_S n_H^2}{\kappa_H n_S^2} \tanh(\gamma_s a) \quad (6)$$

and $\phi = \arctan[(\gamma_C n_H^2)/(\kappa_H n_C^2)]$.

Once there are all the parameters defined and the electric

field has an analytical equation, the next step is program a script in MATLAB for solve the transcendent equation and obtain β. In order to find this constant a little script of Matlab is very helpful. First of all, the definition of the function this will return the zero of the transcendental equation (6). Inside this function, all the transverse parameters have been defined in function of this unknown beta, and then the terms at the left and right of the equality, the subtracting of the left minus right term gives the zero and consequently, the β parameter.

Next step is to call this function and introduce the necessary elements like geometry and material parameters (geometry: a,b; material: n_H, n_S, n_C), and a beta vector formed by range values between the minimum and the maximum of β, which is defined as $\beta_{min} = k_0 n_S$, $\beta_{max} = k_0 n_H$.
With this constant it is trivial to determinate the other transverse parameters and then plot E_x. The figure 3b shows the electric field for several values of the slot width. It can be observed that 2·a, is in nanometre ranger.
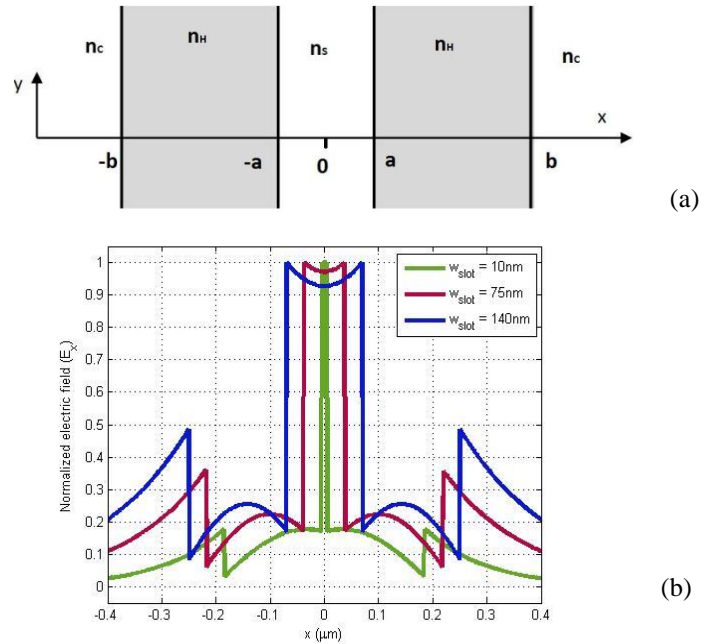

(a)

(b)

FIG. 3: (a) Sketch of the slot waveguide with infinite height. (b) Different normalized transverse electric field distribution for slot-waveguide at $\lambda_0 = 1.55\ \mu m$, with $n_H = 3.48$ (Silicon), $n_s = n_c = 1.44$ (SiO$_2$), $a = \frac{w_{slot}}{2}\ nm$ and $b = (a + 180)nm$.

From equation (3) the electric field undergoes a large discontinuity at $x = \pm a$, in the limit of the slot, which results is a field enhancement in the low-index region, and the e-field immediately inside the slot is n_H^2/n_s^2 times higher than that inside the guide. This ratio is approximately 6 for a Si-SiO$_2$ interface.

These types of slot-waveguides are used in biosensors applications, more than optical communications, because they present high sensitivity than other structures. Sensitivity

$$E_x = A \begin{cases} \dfrac{1}{n_S^2} \cosh(\gamma_S x) & |x| < a \\[2mm] \dfrac{1}{n_H^2} \cosh(\gamma_S a) \cos[\kappa_H(|x| - a)] + \dfrac{\gamma_S}{n_S^2 \kappa_H} \sinh(\gamma_S a) \sin[\kappa_H(|x| - a)] & a < |x| < b \\[2mm] \dfrac{1}{n_C^2} \left\{ \cosh(\gamma_S a) \cos[\kappa_H(b - a)] + \dfrac{n_H^2 \gamma_S}{n_S^2 \kappa_H} \sinh(\gamma_S a) \sin[\kappa_H(b - a)] \right\} \exp[-\gamma_C(|x| - b)] & |x| > b \end{cases} \quad (3)$$

is the change in some optical parameter in front to refractive index.

In evanescent wave sensor, the evanescent wave (100 nm) is in contact with external medium and the local refractive index change the propagation constant. In slot waveguides the biolayer is in the same place where the propagation field is localized, and the modification of propagation conditions is strong than in the previous case [7]. The sensitivity of these devices range is 300-400nm/RIU (Refractive Index Unit) in front of 70nm-100nm/RIU in non-slot sensors. The value is the shift of the resonant wavelength when these slot waveguides are part of a more complex device, a ring resonator [7].

III. SLOT-WAVEGUIDE SIMULATION

For a real study and design of this slot structures, a 3D analysis must be done**.** With the aid of COMSOL multiphysics, finite difference time domain method (FDTD) uses a brute force discretization of Maxwell's equations. The structure is discretized using a uniform grid and the derivatives in Maxwell's equations are replaced by finite differences. Different simulations will be made to see the percentage of power confined in the slot with different width w_{slot}.

This program allows define of electromagnetic wave study and then build the geometry, as well as the refractive index (n) and dielectric constant (κ) of the materials that form the guide and the cover. Besides this, the mesh of simulation can be controlled manually, defining which will be the maximum and the minimum element size. This mesh has been chosen as small as possible in order to solve accurate the electric field distribution inside the small slot widths. However using more grid points results in longer calculation times. The grid size also imposes an upper limit on the time step that can be used, because of stability requirements. Then, the last parameter to configure is the effective mode index according to which the simulation searches modes around.

To do this task better, the definition of a parameter that will be the center of guide position is a good way to optimize the simulation time. Then, there are an option to run the simulation with parametric sweep, which will be defined among a start and final value and number of steps.

In this work, the device consists of a two guides identically, and their widths are 400 nm and 300 nm for height. The slot-waveguide is separated by 10nm (figure 4) and increased in different steps values to finish at $w_{slot} = 600\ nm$ [8].

The values used to define the refractive index (n) of materials that compose the waveguide and the wavelength propagation (λ) was:

n_s (substrate)	n_c (cover)	n_H (guide)	λ (μm)
1.44	1.44	2	1.4

TABLE 1: Values of the device for symmetrical case.

The substrate and cover were made of SiO_2, and the rails were of Si_3N_4. The device sensor was probed at a wavelength around 1.4 μm, which is typically used in telecomm applications (O-band) and leads to lower water optical

absorption than that at the other common telecom wavelength, 1.55 μm.

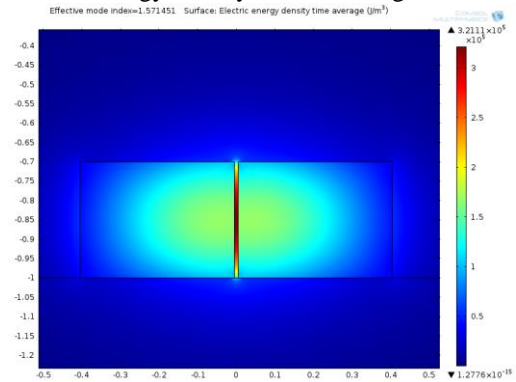It is easy to see in figure 4 that the region of slot contain higher electric energy density than in waveguides.

FIG. 4: COMSOL simulation for energy density of electric field for $w_{slot} = 10\ nm$.

Progressively, the slot width has been increased and the central lobe of the fundamental mode appears in both guides. Furthermore, the electric energy density in the slot decreases but it remains in the external face of the guides. If the slot increases to the final step, $w_{slot} = 400$ nm, the result can be seen in figure 5.
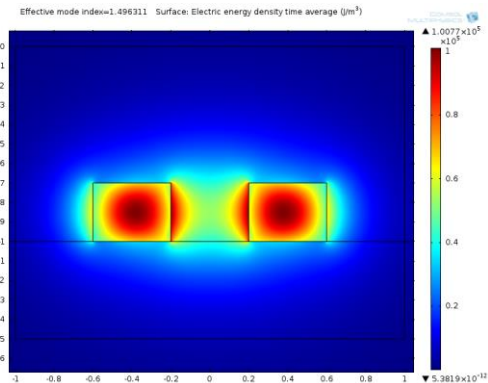

FIG. 5: COMSOL simulation for energy density of electric field for $w_{slot} = 400\ nm$.

Now the lobes were clearly and the intensity at the slot seems to be lower. This occurs because the coupling is present when the slot region is much smaller than the characteristic decay length inside the slot ($w_{slot} \ll \gamma_s$), the field remains high all across the slot. Conversely, if they (slot and wavelength) are the same order size, the slot-waveguide effect disappears and the propagation of the electromagnetic wave was by the guides, and the intensity in the slot diminishes.

Once the simulated was finished, all data was exported to a *.txt* file and processed by different Matlab scripts in order to obtain information about slot-waveguide characteristics. One of them is the electric field distribution (figure 6a), it has the same performance observed in previous theoretical analysis (figure 3b), but the discontinuity of the electric field is lower as a result due to the new ratio from $n_H^2/n_s^2 \approx 2$.

As a result of the electric field enhancement in the slot, the optical intensity there is also much higher than that in the high-index region. In figure 6b can be seen the optical power

P_{slot} and average optical intensity $I_{slot} = P_{slot}/(hw_s)$ inside the slot (where h is the height of the guide) as a function of its width w_s. Both of them are normalized with the respect to the total waveguide optical power. Light propagation in the slot waveguide shows a much higher intensity than that achievable with conventional waveguides.

For an SiO_2-air platform, the highest normalized average intensity is less than $1.1 \ \mu m^{-2}$ for an optimal cross section of 900x500 nm, this is about 5 or 6 times lower than that for the present slot waveguides with an $w_{slot} \approx 50 \ nm$. As well, the devices as antiresosant reflection optical waveguides and photonic crystals waveguides can hardly exceed $1 \ \mu m^{-2}$ at a telecom wavelength, due to the limitation of the low-index core size, because it must be larger than half of the wavelength in the low-index material.
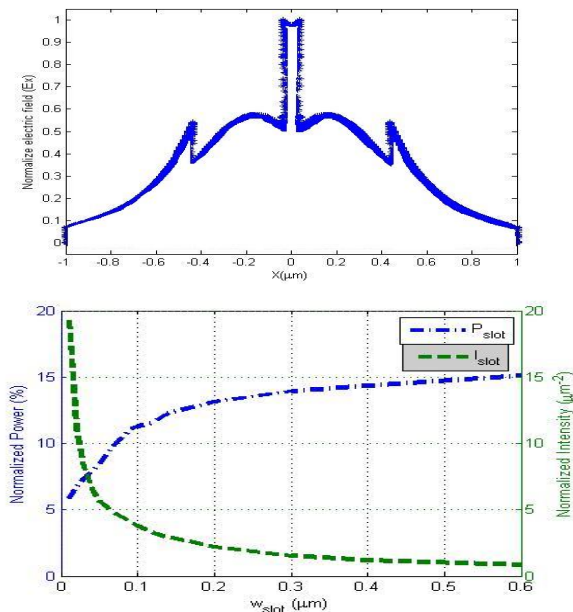
(a)

(b)

FIG. 6: Characterization of slot-waveguide results from COMSOL simulation, (a) electric field distribution for $w_{slot} = 75 \ nm$. (b) Normalized optical power in slot P_{slot} and normalized average optical intensity in slot I_{slot}, for the fundamental TE mode of the slot waveguide.

Other parameter that has been simulated is the wavelength dependence for P_{slot} and I_{slot} (figure 7). This slot-waveguide structure presents very low wavelength sensitivity because there is no interference effect involved in the guiding and confinement mechanism. Then it can be seen that for a wavelength span of 500nm, P_{slot} and I_{slot} vary around 10%.
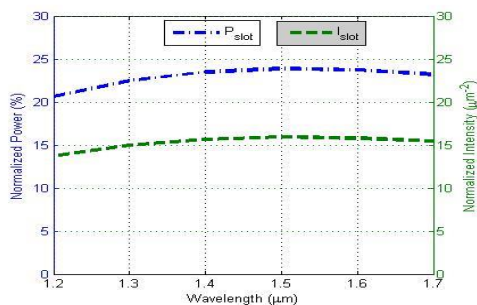
FIG. 7: Wavelength dependence for normalized optical power P_{slot} and normalized optical intensity I_{slot} in the slot with $w_s = 50 \ nm$.

IV. WAVEGUIDE FABRICATION

A. Nano-lithography

The previous devices are produced with a lithography called Electron Beam Lithography (EBL). It consists in a focused beam of electrons to make custom shapes on a surface covered with an electron sensitive film named resist. The electron beam changes the chemical properties of the resist enabling selective removal of either the exposed regions of the resist by immersing it in a developer.

EBL has a principal advantage front other techniques and it is that it does not need a mask to carry out the task because it can draw directly the pattern wanted at the substrate with sub-micrometre resolution, guided with electromagnetic fields serving as a focus lens. Due to the relation of resolution front wavelength $R \sim 1/\lambda$, and $\lambda_{elec.} \ll \lambda_{opt. \ light}$. This is the reason that the EBL must be used for nanometric patterns at the slot-waveguides.

B. Photo-lithography

Photolithography is a process to selectively make a pattern on a substrate. It uses UV light to transfer a pattern from a mask to a light-sensitive chemical called photo resist, it is like the previous resist used in electron beam lithography, but in this case, this is photo sensitive. For this process it is been used a negative photo resin, SU8-10, then the part of the resin that is exposed to light will harden and the other part washed away. The photo lithography consists of a set of steps where the resist transform into a pattern wished. The process steps are [9]:

1. Pre-treatment: This is a process of cleaning and making the substrate ready for lithography. The cleaning consists in ultrasonic baths of acetone for 6 minutes and in isopropanol for 10 more minutes.

2. Spin coat: To deposit a uniform layer of controlled thickness of photo resin on the substrate, a spin coater is used. The substrate is held in place by vacuum, and a chemical resin in applied by pipette. The spin coater then spins at controlled speed, acceleration and time till the required thickness is achieved. For this work three samples has been done at 1000 rpm, 2000 rpm and 3000 rpm for nominal thickness of 30 μm, 15 μm and 10 μm respectively.

3. Soft bake: In this step, the sample is submitted at medium temperature in hot plates, where a heat treatment is done to improve adhesion between resin and substrate: 2 minutes at $T = 65°C$ and 6 minutes at $T = 95°C$.

4. Exposure: Then the sample is covered with the mask and exposed under a UV light for change the conformation of the chemical bonds: 20 seconds of exposure.

5. Post-exposure bake: A new heat treatment at the hot-plate to reduce standing waves from constructive and destructive interference of the light: 2 hours of post-exposure relaxation time.

6. Develop: The sample is immersed into chemical solution (which depends on the resist used) and it dissolves the soft part of the photo resin: 5 minutes of immersion.

7. Hard bake: last part is a new heat treatment at higher temperature, to ensure that the resin has a good adhesion in the substrate.

When all the process has been done, the result is dielectric waveguide with a pattern like figure 8.

FIG. 8: The left picture is the acetate mask and at the right it can be seen the pattern of SU8-10 above the borosilicate crystal.

C. Prism Coupling

Prism coupling is a method of analysis that involves coupling light into the layered being studied, in this case, the SU8 waveguide. The coupling takes place when total internal
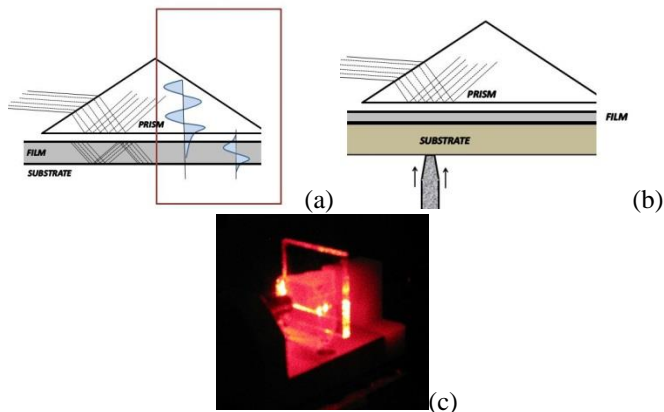

(a)

(b)

(c)

FIG. 9: a) Schematic of coupling light into the waveguide. b) Illustration of external pressure to reduce the distance that the evanescent wave has to travel. c) Photo of experimental prism coupling in a planar waveguide without pattern.

reflection is evidenced at the base of the prism and the evanescent wave that appears in the external medium of the prism can reach the waveguide (figure 9a). To achieve this last requirement and reduce the distance between the prism and the waveguide, an external pressure in a localized point is needed [10]. The result of coupling can be seen at figure 9c. The prism coupler can be used to determine the refractive index and the thickness of a light-guiding thin film as a inverse engineering process. The number of modes found in our samples are: more than 30 modes (59), approximately 25 (29) and 18 (19) for the 30 μm, 15 μm and 10 μm respectively, values near to the theoretical ones (in brackets) after solving the slab waveguide equation.

V. CONCLUSIONS

In this work we have analyzed an emerging type of waveguide, slot waveguides, characterized by a strong of confinement of light in the low refractive index medium. Because of this, these structures present the characteristic of high sensitivity for biochemical sensors.

Future work will be focused in the design of more complex structures, as multiple parallel waveguides or pillars arrays and analyzing the spectral reflectance, and the calculus of sensitivity in front to refractive index.

Also the optimization of fabrication process of waveguides in polymers in the Clean Room of Faculty of Physics will be intensified, including optical techniques for thin film characterization.

_____

[1] Lucas B. Soldano *et. al.*, «Planar Monomode Optical Couplers Based on Multimode Interference Effects,» *J. Lightwave Technol.*, Vol. 10, pp. 1843-1850, 1992.

[2] Haihua Xu *et. al.*, «Silicon optical modulator with integrated grating couplers based on 0.18-μm complementary metal oxide semiconductor technology,» *Opt. Eng.*, Vol 50, 044001, 2011.

[3] B Sepúlveda *et. al.*, «Optical biosensor microsystems based on the integration of highly sensitive Mach–Zehnder interferometer devices,» *J. Opt. A: Pure Appl. Opt.*, Vol. 8, pp. 8561-8566, 2006.

[4] Carlos Angulo Barrios, «Optical Slot-Waveguide Based Biochemical Sensors,» *Sensors*, Vol. 9, pp. 4751-4765, 2009.

[5] Pilar Rodríguez Franco, «Design and functionalization of Optical Resonant Structures for biological applications,» *Master Thesis*, 2011.

[6] Vilson R. Almeida *et. al.*, «Guiding and confining light in void nanostructure,» *Opt. Lett.*, Vol. 29, pp. 1209-1211, 2004.

[7] Carlos A. Barrios *et. al.*, «Label-free optical biosensing with slot-waveguides,» *Opt. Lett.*, Vol. 33, pp. 708-710, 2008.

[8] Carlos A. Barrios *et. al.*, «Demonstration of slot-waveguide structures on silicon nitride / silicon oxide platform,» *Opt. Express*, Vol. 15, pp. 6846-6856, 2007.

[9] Sami Franssila, Introduction to Microfabrication, John Wiley & Sons, 2004.

[10] P. K. Tien and R.Ulrich, «Theory of Prism-Film Coupler and Thin-Film Light Guides,» *J. Opt. Soc. Am.*, Vol. 60, pp. 1325-1337, 1970.